



Cite this: DOI: 10.1039/d1mh00811k

Received 21st May 2021,
Accepted 6th July 2021

DOI: 10.1039/d1mh00811k

rsc.li/materials-horizons

Cucurbituril-activated photoreaction of dithienylethene for controllable targeted lysosomal imaging and anti-counterfeiting†

Guoxing Liu,^a Xiufang Xu,^a Xianyin Dai,^a Chunhui Jiang,^a Yu Zhou,^a Lei Lu^c and Yu Liu^{*,a}

Supramolecular macrocycle-mediated photoreaction has been a research hotspot recently. Herein, we fabricated a photo-responsive intelligent supramolecular assembly that consisted of a water-soluble dithienylethene derivative (DTE-MPBT) and cucurbit[*n*]urils (CB[*n*]). Importantly, CB[*n*], especially CB[8], could act as activators and trigger conformational alteration of the arm parts (typical molecular rotors) of DTE-MPBT, achieving dual functions, *i.e.* high-efficiency visible-light-cyclization reaction of the DTE core and fluorescence enhancement of DTE-MPBT, resulting in the formation of a dual visible light-driven fluorescent switch. These unexpected discoveries prompted the supramolecular assembly to be applied to dual-visible-light-controlled targeted lysosomal imaging and QR code information recognition. Moreover, the solid-state assembly exhibited more outstanding fluorescence and visible-light-switched fluorescence performance because of the host-guest-induced aggregation synergistic effect, showing fascinating applications, such as light-manipulative data storage and anti-counterfeiting. In brief, we unprecedentedly adopted a supramolecular strategy of “killing two birds with one stone”, *i.e.* assembly-activated photochromism (AAP) and assembly-activated emission enhancement (AAEE), to fabricate dual-visible-light-driven fluorescent switches, which show promising application prospects in biomimetic smart nanomaterials based on supramolecular self-assembly systems.

Introduction

Enzyme-catalyzed reactions are ubiquitous in living activities. Natural enzymes are a class of biomacromolecules that play

New concepts

Supramolecular macrocycles can act as artificial enzymes and catalyze given organic photochemistry, arousing widespread research interest. In this work, a photo-responsive intelligent supramolecular assembly that consisted of a water-soluble dithienylethene (DTE) derivative and cucurbit[*n*]urils (CB[*n*]) was constructed through host-guest complexation. To our astonishment, CB[*n*], especially CB[8], could activate high-efficiency visible-light-cyclization reaction of the DTE core and dramatic fluorescence enhancement of the DTE derivative through conformational modulation of its arm parts (typical molecular rotors) encapsulated by CB, leading to the formation of a dual visible light-driven fluorescence switch. The supramolecular assembly was further applied to visible-light-controlled targeted lysosomal imaging and QR code information recognition. In addition, the solid-state assembly displayed more strong fluorescence and visible-light-driven fluorescence switch performance because of the host-guest-induced aggregation synergistic effect, and was further applied in light-manipulative data storage and anti-counterfeiting. Therefore, the study provided a new and simple strategy of “killing two birds with one stone”, *i.e.* assembly-activated photochromism and assembly-activated emission enhancement, to design and prepare dual-visible-light-driven fluorescent switches through conformational modulation, promoting the development of biomimetic smart nanomaterials based on supramolecular self-assembly.

indispensable roles in biological systems,¹ which can provide a binding pocket to encapsulate a substrate and catalyze a specific reaction accordingly.² In an effort to mimic the structure and functionality of enzymes, supramolecular chemists have subtly fabricated a series of artificial macromolecules with cavities as biomimetic enzymes to catalyze organic chemical reactions and photodegradation of organic pollutants, such as organic-metal cages, crown ethers, cyclodextrins, cucurbiturils, pillararenes, calixarenes, molecular baskets, and octa acid.²⁻¹³ Among these macromolecules with holes of specific sizes, cucurbit[*n*]urils (CB[*n*]), a unique class of macrocyclic hosts with stiff cavities, can accommodate positively charged guests or charge-transfer complexes through hydrophobic and electrostatic interaction to form stable host-guest complexes. Although multifarious applications of CB[*n*] have been achieved, such as

^a College of Chemistry, State Key Laboratory of Elemento-Organic Chemistry, Nankai University, Tianjin 300071, P. R. China. E-mail: yuliu@nankai.edu.cn

^b College of Science, Henan Agricultural University, Zhengzhou, Henan 450002, P. R. China

^c College of Information Science and Engineering, Henan University of Technology, Zhengzhou 450001, P. R. China

† Electronic supplementary information (ESI) available: Characterization, other supplementary figures and calculations. See DOI: 10.1039/d1mh00811k

molecular containers,¹⁴ cooperative assembly,¹⁵ molecular machines,^{16,17} supramolecular-organic frameworks,^{18–20} photo-responsive smart materials,^{21–25} and supramolecular photosensitizers,^{26,27} utilization of CB[n] as activators to trigger organic reaction *via* catalysis or synergistic effects has been less explored.^{28–30} Moreover, to the best of our knowledge, CB[n]-activated photoreaction by conformational modulation has been highly underexplored.

Dithienylethene derivatives (DTEs), a class of captivating photochromic molecules, generally undergo cyclization and cycloreversion stimulated using ultraviolet light (high energy) and visible light (low energy), respectively.^{31–34} Dual-visible-light photochromic DTEs are more desirable and would have more valuable applications attributed to avoiding the use of UV light, which has serious shortcomings, for example, causing damage to cells and tissues. A few endeavors have been made to fabricate visible-light photochromic DTEs, including covalent chemical modification, metal coordination, upconverting nanoparticles and triplet-sensitization;^{35–38} however, the research is still in its infancy and new strategies are urgently needed.

Herein, we employed a “killing two birds with one stone” strategy, *i.e.* assembly-activated photochromism (AAP) and assembly-activated emission enhancement (AAEE), to construct dual-visible-light-driven supramolecular fluorescent switches. Water-soluble dithienylethene-bridged-3-methyl-2-phenylbenzo[*d*]thiazol-3-ium (DTE-MPBT), where two typical fluorescent molecular rotors were modified on the DTE skeleton, was ingeniously designed. As illustrated in Fig. 1, MPBT and DTE were the modulatory site and active site, respectively. CB[n], especially CB[8], as activators can tightly encapsulate the modulatory sites to form a supramolecular assembly, and thus activate photocyclization of DTE (active site).

Results and discussion

Construction and characterization of the DTE-MPBT ⊂ CB[8] assembly

Water-soluble DTE-MPBT was successfully synthesized through several simple steps, as shown in Scheme S1 (ESI†). The condensation reaction of **1** with **2** gave compound **3**, and subsequent methylation and ion exchange afforded DTE-MPBT. Furthermore, comprehensive characterization results such as those of ¹H NMR, ¹³C NMR and HR-MS are provided in the ESI.†

We found that CB[8] with a stiff cavity as a host could assemble spontaneously with DTE-MPBT to form a supramolecular assembly (DTE-MPBT ⊂ CB[8]) in water. The assembling behaviors were next studied in detail. The optimum binding stoichiometric ratio was verified using a Job plot, where a maximum peak at a molar ratio of 0.5 was observed, indicating a 1:1 host-guest complex stoichiometry (Fig. S1, ESI†). After confirming the binding stoichiometry, the complex stability constant (K_s) was calculated as $3.19 \times 10^7 \text{ M}^{-1}$ at 25 °C using a nonlinear least-squares curve-fitting method by analyzing the sequential changes in the fluorescence intensity of DTE-MPBT in the presence of varying

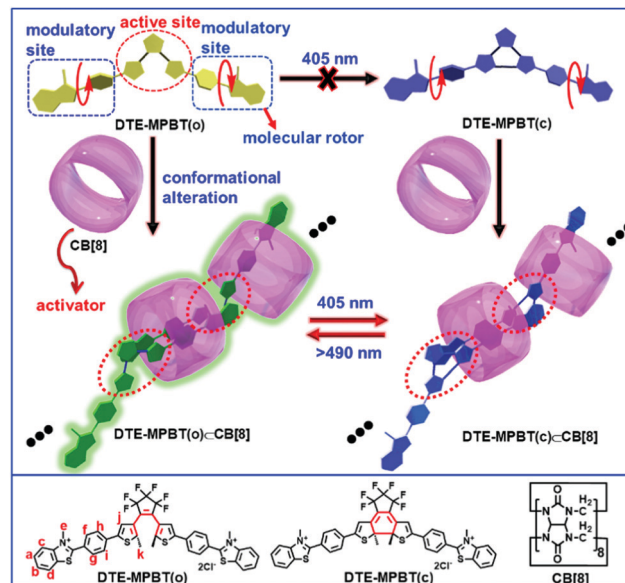


Fig. 1 Chemical structures, assembling pattern, and assembly-activated photochromism of the host and guest. The proposed assembling pattern and visible-light-driven switching mechanism of the assembly DTE-MPBT ⊂ CB[8], and the chemical structures of DTE-MPBT and CB[8].

concentrations of CB[8] (Fig. S2, ESI†).³⁹ To validate the assembly model, the nuclear magnetic titration and contrast experiment were then performed as shown in Fig. S3 and S4 (ESI†). An apparent upfield shift for the resonance of the benzene ring protons (H_{f-i}) adjacent to thiophene and methyl protons (H_c) in thiazol-3-ium and a downfield shift for the benzene ring (H_{a-d}) at the end and thiophene (H_j) were observed. Moreover, half methyl protons connected to thiophene were shifted downfield, and the other half remained unchanged, implying a dynamic inclusion of CB[8] into the guest. In addition, the NOSEY spectrum in Fig. S5 (ESI†) revealed hydrogen correlation between H_k and H_{c-d} , suggesting that there is an interaction between the head and tail of the half guest with the tail and head of another half guest (Fig. S5, ESI†). Moreover, a reference compound, *i.e.* thiophene-modified 3-methyl-2-phenylbenzo[*d*]thiazol-3-ium (T-MPBT) without hexafluorocyclopentene, was prepared to confirm our above speculation. As expected, the resonances for half thiophene ring and benzene ring protons (H_j , H_k , H_c and H_i) at the end of the T-MPBT were shifted upfield, and those of the other half still remained in their original positions, which were consistent with the aforementioned phenomena (Fig. S6, ESI†). The above evidence jointly revealed that there is a dynamic inclusion mechanism between T-MPBT and CB[8], as displayed in Fig. S7 (ESI†). Based on these outcomes, a reasonable assembling pattern of DTE-MPBT and CB[8] was proposed as illustrated in Fig. 1. Moreover, intuitive proof of the assembling morphology was provided by transmission electron microscopy (TEM), where many nanofibers with an average width of 4.8 nm were presented, indicating a feasible secondary aggregation of several linear supramolecular assemblies (Fig. S8, ESI†). Furthermore, the DLS result showed an effective hydrodynamic diameter of about 473.9 nm, implying the formation of nanoaggregates (Fig. S9, ESI†). Further evidence came from 2D

DOSY spectra. As shown in Fig. S10 and Table S1 (ESI[†]), the average diffusion coefficients of CB[8], DTE-MPBT and DTE-MPBT⊂CB[8] were $3.22 \times 10^{-10} \text{ m}^2 \text{ s}^{-1}$, $3.11 \times 10^{-10} \text{ m}^2 \text{ s}^{-1}$ and $1.55 \times 10^{-10} \text{ m}^2 \text{ s}^{-1}$, respectively. By simplistically assuming the complexes as hydrodynamically spherical, the average degree of supramolecular polymerization can be estimated from the obtained diffusion coefficients according to the Stokes–Einstein equation ($D = k_B T / (6\pi\eta R)$).⁴⁰ The average size of the DTE-MPBT⊂CB[8] complex is 9.0 times larger than that of CB[8], implying the formation of large-size supramolecular polymers. Subsequently, we measure the diffusion coefficients of DTE-MPBT⊂CB[8] with two different concentrations (1 mM and 0.5 mM). The average diffusion coefficient of the assembly was obviously decreased from $1.73 \times 10^{-10} \text{ m}^2 \text{ s}^{-1}$ to $1.55 \times 10^{-10} \text{ m}^2 \text{ s}^{-1}$, when its concentration was changed from 0.5 mM to 1.0 mM, which implied that the polymerization degree of the supramolecular assembly was increased with the increase of its concentration (Fig. S11 and Table S2, ESI[†]).

Assembly-activated photochromism (AAP)

Benefiting from the introduction of the dithienylethene unit, the photochromic properties of the assembly and guest were next investigated. Firstly, UV-vis absorption spectra of the open forms of the guest (DTE-MPBT(o)) and assembly (DTE-MPBT(o)⊂CB[8]) were measured. To our excitement, the absorption maximum of the guest exhibited a dramatic bathochromic shift by 83 nm

(from 320 nm to 403 nm) and the molar absorption coefficient (ϵ) at 403 nm was increased by a factor of 6.3 (from $7.5 \times 10^3 \text{ L mol}^{-1} \text{ cm}^{-1}$ to $4.8 \times 10^4 \text{ L mol}^{-1} \text{ cm}^{-1}$) with the addition of 1 eq. CB[8], indicating that assembling behavior occurred and visible-light-triggered cyclization reaction was probably achieved (Fig. 2a). The apparent changes in the absorption and color of the solution (from colorless to yellow, as shown in Fig. 2a, inset) were probably attributed to the conformational alteration of DTE-MPBT from a twisted to flat structure and the formation of an intermolecular charge transfer (ICT) complex in the above process. As we predicted, when the assembly was irradiated with 405 nm visible light, the absorption maximum of DTE-MPBT(o)⊂CB[8] at 403 nm decreased, and a new absorption peak at 671 nm emerged and increased, accompanied by the appearance of three isosbestic points (287 nm, 372 nm and 473 nm) (Fig. 2b). Simultaneously, the solution color changed from yellow to green (Fig. 2b, inset). Accordingly, the aforementioned phenomena altogether indicated the production of a new complex, *i.e.* the closed form of the supramolecular assembly (DTE-MPBT(c)⊂CB[8]). Irradiation of the resultant sample with >490 nm light resulted in the recovery of the original state (from the closed-form of the assembly to its open-form). The photocyclization quantum yield (Φ_{c-o}) and photocycloreversion quantum yield (Φ_{c-o}) of DTE-MPBT were determined to be 0.41 and 0.0011, respectively, which make it have the potential for application in optical memory storage

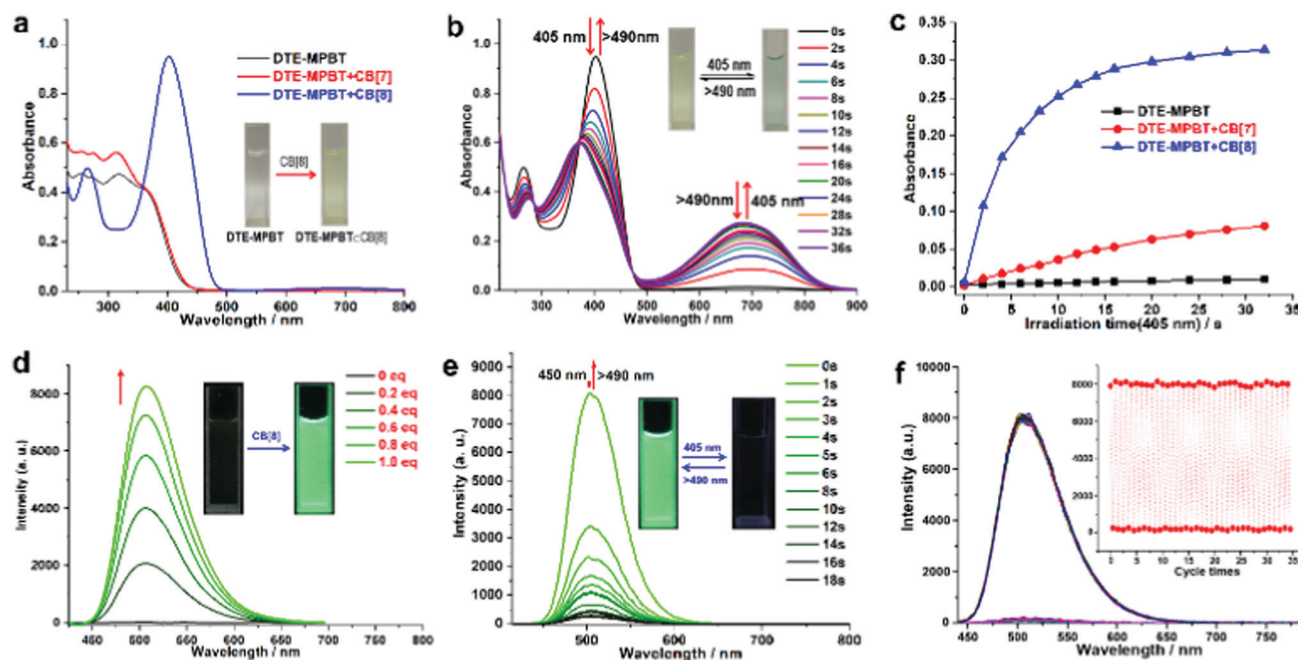


Fig. 2 (a) The UV-vis absorption spectra of DTE-MPBT before and after addition of CB[7] and CB[8]. (b) UV-vis absorption spectral changes of DTE-MPBT⊂CB[8] upon irradiation with alternate 405 nm and >490 nm light. (c) The variation of the absorbance at 620 nm (DTE-MPBT), 630 nm (DTE-MPBT⊂CB[7]₂) and 671 nm (DTE-MPBT⊂CB[8]) with irradiation time using 405 nm light ([CB[7]] = 2 [DTE-MPBT] = 2 [CB[8]] = $4 \times 10^{-5} \text{ M}$). (d) Fluorescence spectral changes of DTE-MPBT upon continuous addition of CB[8] (0–1.0 eq.) in water; inset: Fluorescence photographs of DTE-MPBT and the assembly DTE-MPBT⊂CB[8], under 365 nm UV light. (e) Fluorescence spectral changes of the DTE-MPBT⊂CB[8] assembly upon irradiation at alternate 405 nm and >490 nm light; inset: the alteration of fluorescence photographs of the DTE-MPBT⊂CB[8] assembly upon irradiation with alternate 405 nm and >490 nm visible light. (f) The reversibility of fluorescence switching for DTE-MPBT⊂CB[8] monitored at 505 nm over 35 cycles upon alternating irradiation with 405 nm and >490 nm visible light. ([DTE-MPBT] = [CB[8]] = $5 \times 10^{-6} \text{ M}$, λ_{ex} = 406 nm; slit = 1.0, 2.5).

Table 1 Photochromic parameters of the guest DTE-MPBT and the assemblies DTE-MPBT⊂CB[8] and DTE-MPBT⊂CB[7]₂ in aqueous solution ($c = 2 \times 10^{-5}$ M, 298 K)

Complex	$\lambda_{\max}/\text{nm}^a$ ($\epsilon \times 10^{-4}$)	$\lambda_{\max}/\text{nm}^b$ ($\epsilon \times 10^{-4}$)	Φ^c
	(Open)	(PSS)	$\Phi_{\text{o-c}}$ $\Phi_{\text{c-o}}$
DTE-MPBT	362 nm (3.91)		
DTE-MPBT⊂CB8	402 nm (4.83)	671 nm (1.36)	0.41 0.0011
DTE-MPBT⊂CB7 ₂	368 nm (4.37)	630 nm (1.94)	0.08 0.0017

^a Absorption maxima of open-ring isomers. ^b Absorption maxima of closed-ring isomers. ^c Quantum yields of open-ring ($\Phi_{\text{o-c}}$) and closed-ring isomers ($\Phi_{\text{c-o}}$), respectively.

(Table 1).^{41–45} In addition, the photocyclization conversion yield was determined to be 92% by NMR (Fig. S12, ESI[†]). In contrast, only DTE-MPBT exhibited inert photocyclization properties upon irradiation with 405 nm visible light, as shown in Fig. S13, (ESI[†]). Therefore, CB[8] could activate high-efficient visible-light-cyclization reaction of DTE-MPBT through assembly-caused conformational alteration. To further confirm our viewpoint, we then investigated the influence of another homogeneous CB, *i.e.* CB[7], on the photochromism of DTE-MPBT, whose cavity is smaller than that of CB[8]. Initially, we studied the assembling behavior of DTE-MPBT with CB[7] in detail. As shown in Fig. S14, (ESI[†]), their optimum binding stoichiometric ratio was verified using a Job plot at a molar ratio of 0.33 with a maximum peak, indicating a 2 : 1 host–guest binding stoichiometry. After confirming the binding stoichiometry, the complex stability constants (K_s) of DTE-MPBT and CB[7] were calculated to be $K_{S1} = 2.66 \times 10^4 \text{ M}^{-1}$ and $K_{S2} = 1.62 \times 10^6 \text{ M}^{-1}$ at 25 °C by analyzing the sequential changes in absorbance of DTE-MPBT at 363 nm along with varying concentrations of CB[7] using a nonlinear least-squares curve-fitting method (Fig. S15 and S16, ESI[†]). In contrast to the ¹H NMR spectra in Fig. S17 (ESI[†]), the resonances of segment protons ($H_{\text{a-i}}$) for DTE-MPBT were all obviously shifted upfield and a downfield shift for methylthiophene ($H_{\text{j-k}}$) was observed inversely, indicating the formation of the DTE-MPBT⊂CB[7]₂ assembly and the rationality of the proposed assembly model (Fig. S18, ESI[†]). After clarifying the assembling model of DTE-MPBT⊂CB[7]₂, the photocyclization reaction of the assembly was subsequently investigated. As expected, the conformational modulation of CB[7] on DTE-MPBT also activated visible-light-cyclization of the photochromic molecule (Fig. S18, ESI[†]). As shown in Fig. S19 (ESI[†]), the absorbance of DTE-MPBT(o)⊂CB[7]₂ at 368 nm decreased gradually, and a new absorption peak at 630 nm emerged and gradually increased, accompanied by the appearance of three isoabsorptive points at 286 nm, 346 nm and 424 nm, indicating that a new complex, *i.e.* the closed-form of DTE-MPBT⊂CB[7]₂, was generated. Furthermore, the photocyclization conversion yield was calculated as approximately 83% by ¹H NMR (Fig. S20, ESI[†]). The $\Phi_{\text{o-c}}$ and $\Phi_{\text{c-o}}$ of DTE-MPBT⊂CB[7]₂ was determined to be 0.08 and 0.0017, respectively (Table 1). More intuitively, the absorbance variation curves of their closed-forms at their absorption maxima (671 nm for DTE-MPBT⊂CB[8], 620 nm for DTE-MPBT, and 630 nm for DTE-MPBT⊂CB[7]₂) as functions of consecutive irradiation time using 405 nm light (Fig. 2c) revealed the fastest photocyclization

reaction speed for the supramolecular assembly DTE-MPBT⊂CB[8]. In a word, the photocyclization quantum yield, and conversion yield and speed of the DTE-MPBT⊂CB[7]₂ assembly were far inferior to those of DTE-MPBT⊂CB[8]. The reason was probably that MPBT (a typical molecular rotor) as the modulatory site enabled more efficient conformational alteration activated by CB[8] than CB[7], which originated from tighter encapsulation of MPBT within CB[8]. The direct proof was that the binding ability of DTE-MPBT with CB[8] ($K_s = 3.19 \times 10^7 \text{ M}^{-1}$) was dramatically stronger than that of the guest with CB[7] ($K_{S1} = 2.66 \times 10^4 \text{ M}^{-1}$ and $K_{S2} = 1.62 \times 10^6 \text{ M}^{-1}$). Further competent proof was that the fluorescence of DTE-MPBT⊂CB[8] was greatly stronger than that of DTE-MPBT⊂CB[7]₂, implying tighter encapsulation of MPBT within CB[8] compared to CB[7] (Fig. S21, ESI[†]). In a word, the aforementioned observations fully demonstrated that the photocyclization reaction of DTE (active site) could be activated by CB[7], especially CB[8], which acted as an activator to complex with MPBT (modulatory site), as illustrated in Fig. 1. Consequently, we successfully applied an assembly-activated photochromism (AAP) strategy to enable dual-visible-light photochromism in our newly designed system.

Assembly-activated emission enhancement (AAEE)

An interesting phenomenon was that CB[8] also played an important role in enhancing the fluorescence of DTE-MPBT. As displayed in Fig. 2d, the fluorescence intensity of the guest DTE-MPBT at 505 nm was drastically increased by a factor of up to 420 in the presence of 1 eq. CB[8], probably attributed to the conformational alteration and restriction caused by host–guest complexation. Visually, the fluorescence of DTE-MPBT turned into strong green after addition of 1 eq. CB[8], enabling observation with the naked eye (Fig. 2d, inset). Quantitatively, the relative fluorescence quantum yield (Φ_F) was greatly enhanced from 0.27% to 46.2% and the fluorescence lifetime of DTE-MPBT was increased from 1.71 to 2.62 ns in the presence of CB[8] (Fig. S22, ESI[†]). In this system, the guest DTE-MPBT, a typical fluorescent molecular rotor, was encapsulated in the cavity of CB[8] to form a stable supramolecular assembly, and the structure of MPBT in the guest tended to be flat. The twisted intramolecular charge transfer (TICT) state of DTE-MPBT was efficiently changed to the ICT state, leading to dramatic fluorescence enhancement, namely assembly-activated emission enhancement (AAEE).³⁶ To verify our viewpoint, the maximum fluorescence emission intensity of DTE-MPBT at 500 nm was gradually increased as well by a factor of 30 along with continuous addition of CB[7] (Fig. S23, ESI[†]), which also originated from conformational restriction caused by the encapsulation of CB[7]. Indeed, no apparent variation was observed in the presence of 2 eq. of CB[7], also implying 1 : 2 host–guest binding stoichiometry (Fig. S23, ESI[†]). However, the fluorescence of DTE-MPBT⊂CB[7]₂ was greatly weaker than that of DTE-MPBT⊂CB[8] due to the looser encapsulation of the guest in the hole of CB[7]. Hence, the strong fluorescence intensity, high Φ_F and good water solubility of the stable supramolecular assembly DTE-MPBT⊂CB[8] would make it a promising candidate for cell imaging and fluorescence sensing.

Theoretical calculation on AAP and AAEE

The relevant theoretical calculation was performed to verify AAP and AAEE. The proposed assembling model of DTE-MPBT and CB[8] is shown in Fig. 3a, where two 3-methyl-2-phenylbenzo[*d*]thiazol-3-ium moieties from adjacent DTE-MPBT molecules were encapsulated in the cavity of CB[8] and positioned in an antiparallel manner to each other. Then, the optimized geometry of the simplified assembly was obtained through DFT calculation and is shown in Fig. 3b. From the optimized geometry of the assembly, the torsion angles between the benzene ring and benzothiazole of 2-phenylbenzothiazole moieties decreased from 40° in the free guest molecule DTE-MPBT to 13° in the assembly DTE-MPBT=CB[8], indicating the occurrence of the conformational modulation process (Fig. 3b–d). This result revealed that the MPBT section became more planar in the cavity of CB8, and further disclosed that the dramatic fluorescence enhancement of the guest originated from conformational restriction after assembling with CB[8].⁴⁶ The HOMO and LUMO energies of the free guest DTE-MPBT and the assembly DTE-MPBT=CB[8] are also shown in Fig. 3c and d. According to the LUMO–HOMO gaps, the absorption wavelength was calculated to be red-shifted from 426 nm to 437 nm, attributed to the conformational modulation of MPBT. Although the absorption positions were somewhat different from the experimental outcomes, the calculated dramatic absorption spectral red-shift was consistent with the results of the above experiments. This revealed that the intervention of CB[8] lowered efficiently the photocyclization energy of DTE-MPBT(o).

Dual visible light-triggered fluorescence switch

After a sufficient comparison of the fluorescence intensity and photochromic performance of the two assemblies, we selected DTE-MPBT=CB[8] for further research. It was very significant that the DTE-MPBT(o)=CB[8] assembly could act as a dual visible light-driven fluorescent switch. As shown in Fig. 2e, 99%

fluorescence of DTE-MPBT(o)=CB[8] at 505 nm was quenched rapidly upon irradiation with 405 nm visible light for only 18 s. Meanwhile, the relative Φ_F was reduced from 46.2% to 0.62%, and the strong green fluorescence became invisible to the naked eye (Fig. 2e, inset). Nevertheless, the fluorescence intensity and photograph were completely recovered when the assembly was irradiated with >490 nm visible light. Crucially, the above fluorescence switching process could be repeated at least 35 times without any recession, indicating outstanding fatigue resistance (Fig. 2f). Overall, the supramolecular assembly DTE-MPBT=CB[8] could become a uniquely charismatic dual-visible-light-triggered fluorescence switch, which could be operated in aqueous solution.

Dual visible light-controlled lysosomal targeting imaging

The above remarkable peculiarities such as the strong fluorescence, high Φ_F , good water-solubility, dual-visible-light-response and excellent reversibility encouraged us to explore the application of DTE-MPBT=CB[8] in the biological field. A549 cells were selected to be co-stained with the assembly DTE-MPBT=CB[8] and commercially available lysosome staining dye LysoBlue for 4 h in the dark. Subsequently, we employed confocal laser scanning microscopy to investigate the intracellular distribution of the assembly. As shown in Fig. 4c, the merged image of green DTE-MPBT=CB[8] (Fig. 4b) and blue LysoBlue (Fig. 4a) revealed that DTE-MPBT=CB[8] and LysoBlue were completely co-located in the same site, indicating that the fluorescent supramolecular assembly achieved accurately lysosomal targeting imaging in living cells. Meanwhile, the cytotoxicity of the assembly was also evaluated. A549 cells were incubated with the assembly for 24 h, and the cell viability was then examined by MTT assays. When the concentration of the assembly was under 20 μM ($[\text{DTE-MPBT}] = [\text{CB}[8]] = 20 \mu\text{M}$), the toxicity to A549 cells was ignorable completely (Fig. 4d). Furthermore, 293T cells were selected to investigate the cytotoxicity of the assembly on a selection of healthy cells. The result revealed that the toxicity to 293T cells was also fully negligible when the concentration of the assembly was less than 20 μM (Fig. S24, ESI[†]). Photo-controlled lysosomal targeting imaging was further performed using the supramolecular assembly as a result of its reversible dual-visible-light-activated fluorescence switching peculiarity. As shown in Fig. 4e, the strong green fluorescence in lysosomes was quenched upon 405 nm laser irradiation for 2 s, while the complete recovery of the original fluorescence was enabled by subsequent 633 nm laser irradiation for 10 s. The fluorescence quenching time (2 s) was shorter than the one in the previous irradiation experiment (16 s), which was probably attributed to the higher optical power density and lower concentration of the sample distributed in lysosomes. Besides, we performed six irradiation reciprocating experiments, and no apparent decrease of the initial fluorescence intensity was observed, revealing good fatigue resistance for photoswitching lysosomal targeting imaging (Fig. S25, ESI[†]). We reported the first supramolecular smart material with the function of dual visible-light-controlled lysosomal targeting imaging, to the best of our knowledge.

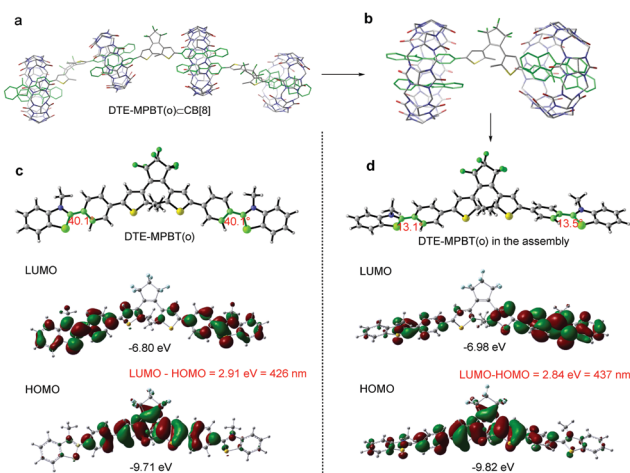


Fig. 3 (a) The proposed model for the assembly DTE-MPBT=CB[8]; (b) optimized geometry of the simplified structure of DTE-MPBT=CB[8]; (c) the structure and orbitals of free DTE-MPBT; and (d) the structure and orbitals of DTE-MPBT with the inclusion of CB[8].

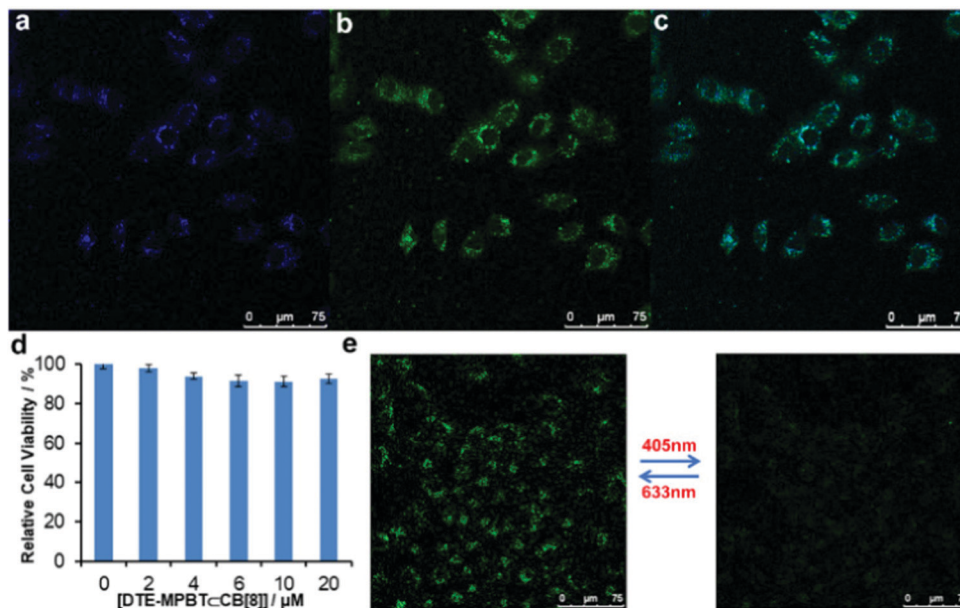


Fig. 4 Confocal fluorescence images of A549 cells co-stained with DTE-MPBT@CB[8] ([DTE-MPBT] = [CB[8]] = 1×10^{-5} M) and LysoBlue (5×10^{-6} M) for 4 h: (a) LysoBlue (Ex. 405 nm, Em. 425 nm); (b) DTE-MPBT@CB[8] (Ex. 405 nm, Em. 505 nm); (c) merged image of (a) and (b); (d) relative cell viabilities of DTE-MPBT@CB[8] at different concentrations; and (e) the variation and reversibility of confocal fluorescence images of A549 cells co-stained with DTE-MPBT@CB[8] in the same region upon alternate 405 nm and 633 nm laser irradiation.

Dual visible light-switched QR code anti-counterfeiting

The fast photo-responsive fluorescence switching properties of DTE-MPBT@CB[8] also encouraged us to further explore its application in anti-counterfeiting and security. In recent years, QR code has emerged more and more frequently in our daily life and brought us a great deal of convenience. Thus, the DTE-MPBT@CB[8] assembly has great potential for application in QR code anti-counterfeiting. To ascertain the possibility of this application, an aqueous solution containing DTE-MPBT@CB[8] was filled in the groove of a 3D model fabricated using a 3D printer. The model showed well-defined QR code under 365 nm UV light (Fig. 5). We could recognize the corresponding website from the QR code using our mobile phones. Subsequently, irradiation of the model with 405 nm light led to fluorescence quenching and the disappearance of the QR code. Crucially, when the resultant sample was irradiated with >490 nm visible light, the original QR code reemerged and was recognized using mobile phones again. The aforementioned process could be repeated many times, which originated from the excellent fatigue resistance of the supramolecular fluorescent photoswitch. With the satisfactory experimental results in hand,

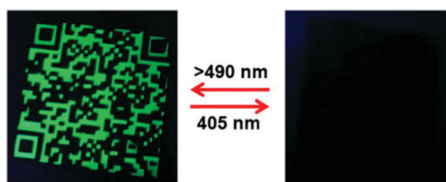


Fig. 5 Dual visible light-switched fluorescent QR code of DTE-MPBT@CB[8].

dual visible-light-triggered reversible information hiding and recognition were successfully performed.

Dual visible light-triggered solid-state fluorescence switching and data storage

Inspired by the above findings, we investigated the solid-state photoluminescence switching and data storage functions of the DTE-MPBT@CB[8] assembly. We performed powder X-ray diffraction of DTE-MPBT, CB[8] and DTE-MPBT@CB[8] powders. As displayed in Fig. S26 (ESI[†]), the XRD spectrum of the DTE-MPBT@CB[8] assembly was apparently different from the ones of the DTE-MPBT guest and the CB[8] host, implying that the supramolecular assembly still maintained the initial host-guest inclusion state in its solid powder. The solid-state DTE-MPBT@CB[8] assembly exhibited immensely strong green fluorescence with the maximum emission peak at 523 nm (Fig. 6a), which displayed an obvious bathochromic-shift of about 18 nm compared to DTE-MPBT@CB[8] in aqueous solution (505 nm). Simultaneously, the absolute fluorescence quantum yield of the solid-state assembly (52.5%) was apparently higher than that of the assembly in aqueous solution (41.7%), as displayed in Fig. S27 and S28 (ESI[†]). The above phenomena were attributed to the formation of a more planar DTE-MPBT structure in solid powder.

Moreover, the fluorescence lifetime of the solid-state assembly was determined as 2.48 ns (Fig. S29, ESI[†]) comparable to that of the solution-state assembly (2.62 ns). Just as we expected, when DTE-MPBT@CB[8] solid powder was irradiated with 405 nm light for only 8 s, the solid-state fluorescence of the assembly at 523 nm was strongly quenched up to 96%, indicating faster photoinduced fluorescence quenching than the sample in aqueous solution

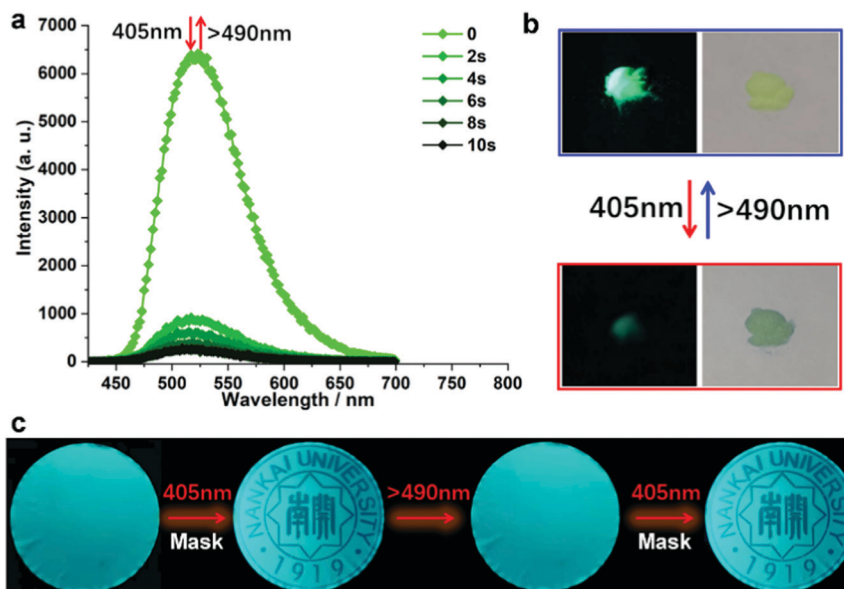


Fig. 6 (a) The variation of fluorescence spectra of the solid-state supramolecular assembly DTE-MPBT \subset CB[8] upon irradiation with 405 nm visible light. (b) The photographs of DTE-MPBT \subset CB[8] solid powder under 365 nm UV light and an incandescent lamp upon alternating 405 nm and >490 nm irradiation. (c) The fluorescence image (the badge of Nankai University) was sequentially recorded onto and erased from the same mixed fiber microporous membrane using different masks with 405 nm irradiation for 8 s and >490 nm irradiation for 20 s, respectively.

(Fig. 6a). Visually, in the above process, the strong green fluorescence became almost invisible to the naked eye, and the color of the solid powder under the incandescent lamp changed from yellow to blue (Fig. 6b). These observations altogether revealed that the open-form of the DTE-MPBT \subset CB[8] assembly was transformed indubitably to its closed-form. Subsequently, irradiation of the resultant sample with >490 nm visible light led to the complete recovery of the fluorescence spectrum, fluorescence image and sample color. In view of the high-efficiency, fatigue-resistant and visible-light photochromism and fluorescence switching characteristics of the assembly, we then tried to develop visible-light-triggered fluorescence patterning application for data storage. We fabricated a solid-state photoluminescent film by soaking a mixed fiber microporous membrane into an aqueous solution containing DTE-MPBT \subset CB[8] (2×10^{-5} M) and subsequently drying it. By exposing the film to the recording visible light ($\lambda = 405$ nm) locally through a specific mask, the pattern of “the badge of Nankai University” could be handily and clearly recorded (Fig. 6c). The formed pattern could be erased by irradiation with $\lambda > 490$ nm visible light. Importantly, the pattern could be consecutively recorded and erased under all-visible-light recording-erasing cycles, and no fluorescence degradation was observed. These results show that DTE-MPBT \subset CB[8] will have promising applications in the future in all visible light-manipulative data storage, anti-counterfeiting and data confidence.

Conclusions

In this work, by imitating the structure and functionality of natural enzymes, assembly-activated photochromism and assembly-activated emission enhancement (killing two birds with one stone) were adopted to construct a dual visible-light-switched

fluorescent supramolecular assembly, where a CB as a macrocyclic host acted as an activator. The water-soluble DTE-MPBT equipped with dithienylethene and a fluorescent molecular rotor was elaborately designed and synthesized. CB[n], especially CB[8], as a modulator could restrict the rotation of MPBT sections (molecular rotor), urging the parts to form intermolecular CT and trend to flat. And then, the absorption maximum of the guest was bathochromically shifted to the visible region, enabling the DTE-MPBT \subset CB[8] assembly to undergo visible light (405 nm)-driven cyclization reaction with high Φ_{o-c} for 0.41 *via* an AAP strategy. Furthermore, the intervention of CB[8] also results in a high-efficiency fluorescence enhancement of DTE-MPBT with Φ_F from 0.5% to 46.2% through an AAEE way. Significantly, the induced strong fluorescence could be highly efficiently switched with two distinct visible light sources (different wavelengths) along with excellent fatigue resistance. To our delight, the resultant supramolecular assembly could be first applied to dual-visible-light-controlled targeted lysosomal cell imaging and QR code information recognition. Simultaneously, DTE-MPBT \subset CB[8] exhibited the particular characteristic of dual-visible-light-triggered solid-state fluorescence switching, and presented the intelligent function of light-manipulative data storage and anti-counterfeiting. The study provided a biomimetic strategy for the construction of dual-visible-light-driven smart supramolecular nanomaterials, which made a unique contribution to the revolution of advanced materials.

Author contributions

Guoxing Liu and Yu Liu conceived the experiments and wrote this paper. Guoxing Liu performed all syntheses and optical measurements. Xiufang Xu, Yu Zhou and Chunhui Jiang

performed the theoretical calculations. Xianyin Dai performed the targeting lysosomal imaging experiment. Lei Lu made the 3D QR code model.

Conflicts of interest

The authors declare no competing financial interests.

Acknowledgements

We thank the National Natural Science Foundation of China (No. 21801063), China Postdoctoral Science Foundation (No. 2018M642767), Science and Technology Foundation of Henan Province (No. 192102210039) and Colleges and Universities Key Research Program Foundation of Henan Province (No. 19A150022) for financial support.

Notes and references

- 1 A. Stank, D. B. Kokh, J. C. Fuller and R. C. Wade, *Acc. Chem. Res.*, 2016, **49**, 809–815.
- 2 Y. Fang, J. A. Powell, E. Li, Q. Wang, Z. Perry, A. Kirchon, X. Yang, Z. Xiao, C. Zhu, L. Zhang, F. Huang and H.-C. Zhou, *Chem. Soc. Rev.*, 2019, **48**, 4707–4730.
- 3 C. Tan, D. Chu, X. Tang, Y. Liu, W. Xuan and Y. Cui, *Chem. – Eur. J.*, 2019, **25**, 662–672.
- 4 Y. Inokuma, M. Kawano and M. Fujita, *Nat. Chem.*, 2011, **3**, 349–358.
- 5 S. Zarra, D. M. Wood, D. A. Roberts and J. R. Nitschke, *Chem. Soc. Rev.*, 2015, **44**, 419–432.
- 6 Y.-X. Wang, Y.-M. Zhang and Y. Liu, *J. Am. Chem. Soc.*, 2015, **137**, 4543–4549.
- 7 V. Ramamurthy and J. Sivaguru, *Chem. Rev.*, 2016, **116**(17), 9914–9993.
- 8 X. Guan, Y. Chen, P. Guo, P. Li and Y. Liu, *Chem. Commun.*, 2020, **56**, 7187–7190.
- 9 S. Guo, X. Liu, C. Yao, C. Lu, Q. Chen, X.-Y. Hu and L. Wang, *Chem. Commun.*, 2016, **52**, 10751–10754.
- 10 N. Kamatham, J. P. D. Silva, R. S. Givens and V. Ramamurthy, *Org. Lett.*, 2017, **19**, 3588–3591.
- 11 S. E. Border, R. Z. Pavlović, L. Zhiquan and J. D. Badjić, *J. Am. Chem. Soc.*, 2017, **139**, 18496–18499.
- 12 Q. Wang, W. Liang, X. Wei, W. Wu, Y. Inoue, C. Yang and Y. Liu, *Org. Lett.*, 2020, **22**, 9757–9761.
- 13 J. Ji, W. Wu, W. Liang, G. Cheng, R. Matsushita, Z. Yan, X. Wei, M. Rao, D.-Q. Yuan, G. Fukuhara, T. Mori, Y. Inoue and C. Yang, *J. Am. Chem. Soc.*, 2019, **141**, 9225–9238.
- 14 H. S. El-Sheshtawy, B. S. Bassil, K. I. Assaf, U. Kortz and W. M. Nau, *J. Am. Chem. Soc.*, 2012, **134**, 19935–19941.
- 15 C. Ke, N. L. Strutt, H. Li, X. Hou, K. J. Hartlieb, P. R. McGonigal, Z. Ma, J. Iehl, C. L. Stern, C. Cheng, Z. Zhu, N. A. Vermeulen, T. J. Meade, Y. Y. Botros and J. F. Stoddart, *J. Am. Chem. Soc.*, 2013, **135**, 17019–17030.
- 16 F. Tian, D. Jiao, F. Biedermann and O. A. Scherman, *Nat. Commun.*, 2012, **3**, 1207–1215.
- 17 H. Yin, R. Rosas, D. Gígenes, O. Ouari, R. Wang, A. Kermagoret and D. Bardelang, *Org. Lett.*, 2018, **20**, 3187–3191.
- 18 K.-D. Zhang, J. Tian, D. Hanifi, Y. Zhang, A. C.-H. Sue, T.-Y. Zhou, L. Zhang, X. Zhao, Y. Liu and Z.-T. Li, *J. Am. Chem. Soc.*, 2013, **135**, 17913–17918.
- 19 M. Pfeiffermann, R. Dong, R. Graf, W. Zajaczkowski, T. Gorelik, W. Pisula, A. Narita, K. Müllen and X. Feng, *J. Am. Chem. Soc.*, 2015, **137**, 14525–14532.
- 20 Y. Chen, F. Huang, Z.-T. Li and Y. Liu, *Sci. China: Chem.*, 2018, **61**, 979–992.
- 21 W. Zhang, Y.-M. Zhang, S.-H. Li, Y.-L. Cui, J. Yu and Y. Liu, *Angew. Chem., Int. Ed.*, 2016, **55**, 11452–11456.
- 22 X.-L. Ni, S. Chen, Y. Yang and Z. Tao, *J. Am. Chem. Soc.*, 2016, **138**, 6177–6183.
- 23 G. Liu, Y.-M. Zhang, C. Wang and Y. Liu, *Chem. – Eur. J.*, 2017, **23**, 14425–14429.
- 24 E.-R. Janeček, J. R. McKee, C. S. Y. Tan, A. Nykänen, M. Kettunen, J. Laine, O. Ikkala and O. A. Scherman, *Angew. Chem., Int. Ed.*, 2015, **54**, 5383–5388.
- 25 F.-F. Shen, Y. Chen, X. Dai, H.-Y. Zhang, B. Zhang, Y. Liu and Y. Liu, *Chem. Sci.*, 2021, **12**, 1851–1857.
- 26 K. Liu, Y. Liu, Y. Yao, H. Yuan, S. Wang, Z. Wang and X. Zhang, *Angew. Chem., Int. Ed.*, 2013, **52**, 8285–8289.
- 27 Y. Liu, Z. Huang, K. Liu, H. Kelgtermans, W. Dehaen, Z. Wang and X. Zhang, *Polym. Chem.*, 2014, **5**, 53–56.
- 28 X. Hou, C. Ke and J. F. Stoddart, *Chem. Soc. Rev.*, 2016, **45**, 3766–3780.
- 29 C. Yang, C. Ke, W. Liang, G. Fukuhara, T. Mori, Y. Liu and Y. Inoue, *J. Am. Chem. Soc.*, 2011, **133**, 13786–13789.
- 30 L. Zheng, S. Sonzini, M. Ambarwati, E. Rosta, O. A. Scherman and A. Herrmann, *Angew. Chem., Int. Ed.*, 2015, **54**, 13007–13011.
- 31 M. Irie, T. Fukaminato, K. Matsuda and S. Kobatake, *Chem. Rev.*, 2014, **114**, 12174–12277.
- 32 D.-H. Qu, Q.-C. Wang, Q.-W. Zhang, X. Ma and H. Tian, *Chem. Rev.*, 2015, **115**, 7543–7588.
- 33 Z. Li, G. Davidson-Rozenfeld, M. Vázquez-González, M. Fadeev, J. Zhang, H. Tian and I. Willner, *J. Am. Chem. Soc.*, 2018, **140**, 17691–17701.
- 34 S. Wang, W. Shen, Y. Feng and H. Tian, *Chem. Commun.*, 2006, 1497–1499.
- 35 D. Bléfer and S. Hecht, *Angew. Chem., Int. Ed.*, 2015, **54**, 11338–11349.
- 36 T. Fukaminato, T. Hirose, T. Doi, M. Hazama, K. Matsuda and M. Irie, *J. Am. Chem. Soc.*, 2014, **136**, 17145–17154.
- 37 J. Xu, H. Volfova, R. J. Mulder, L. Goerigk, G. Bryant, E. Riedle and C. Ritchie, *J. Am. Chem. Soc.*, 2018, **140**, 10482–10487.
- 38 Z. Zhang, W. Wang, P. Jin, J. Xue, L. Sun, J. Huang, J. Zhang and H. Tian, *Nat. Commun.*, 2019, **10**, 4232.
- 39 G. Liu, Y.-M. Zhang, X. Xu, L. Zhang, Q. Yu, Q. Zhao, C. Zhao and Y. Liu, *Adv. Opt. Mater.*, 2017, **5**, 1700770.
- 40 R. Schmidt, M. Stolte, M. Grüne and F. Würthner, *Macromolecules*, 2011, **44**, 3766–3776.
- 41 L. Hou, X. Zhang, T. C. Pijper, W. R. Browne and B. L. Feringa, *J. Am. Chem. Soc.*, 2014, **136**, 910–913.
- 42 Y. Wu, W. Zhu, W. Wan, Y. Xie, H. Tian and A. D. Q. Li, *Chem. Commun.*, 2014, **50**, 14205–14208.

- 43 W. Li, C. Jiao, X. Li, Y. Xie, K. Nakatani, H. Tian and W. Zhu, *Angew. Chem., Int. Ed.*, 2014, **53**, 4603–4607.
- 44 M. Irie, K. Sakemura, M. Okinaka and K. Uchida, *J. Org. Chem.*, 1995, **60**, 8305–8309.
- 45 B. Qin, R. Yao, X. Zhao and H. Tian, *Org. Biomol. Chem.*, 2003, **1**, 2187–2191.
- 46 Y.-M. Zhang, X.-J. Zhang, X. Xu, X.-N. Fu, H.-B. Hou and Y. Liu, *J. Phys. Chem. B*, 2016, **120**, 3932–3940.